J. Wind Eng. Ind. Aerodyn. 98 (2010) 888–894

Contents lists available at ScienceDirect

Journal of Wind Engineering and Industrial Aerodynamics

journal homepage: www.elsevier.com/locate/jweia

An experimental investigation of the recirculation zone formed downstream of a forward facing step

M. Sherry [a,*], D. Lo Jacono [a,b,c], J. Sheridan [a]

[a] Fluids Laboratory for Aeronautical and Industrial Research, Department of Mechanical and Aerospace Engineering, Monash University, Clayton, Victoria 3800, Australia
[b] Université de Toulouse, INPT, UPS, IMFT, Allée Camille Soula, F-31400 Toulouse, France
[c] CNRS, IMFT, F-31400 Toulouse, France

ARTICLE INFO

Article history:
Received 21 October 2009
Received in revised form
3 September 2010
Accepted 8 September 2010

Keywords:
Flow separation
Recirculation zone
Forward facing step
Wind turbine siting

ABSTRACT

An experimental investigation of the recirculation zone formed downstream of a forward facing step immersed in a turbulent boundary layer has been undertaken using particle image velocimetry. Bluff body flow is observed with the fixed separation point located at the leading edge of the step. The recirculation region dimensions are characterised over a range of Reynolds numbers (1400–19 000), with Re_h based on the step height and the free stream velocity. Turbulent perturbations are produced in the free shear layer which develops between the recirculating flow close to the step and the free stream flow. Contour maps of amplification factor, streamwise perturbation velocity and Reynolds stresses are constructed, providing insight into optimal placement of structures within such topographical features. The mechanisms affecting the reattachment distance, namely the turbulent mixing within the boundary layer and the velocity deficit in the boundary layer, are discussed.

1. Introduction

Separating and reattaching flow phenomena are of particular interest for wind engineering applications. One area of wind engineering which has seen rapid development in recent times is wind energy. Wind turbines are commonly sited in the vicinity of topological features such as coastal cliffs and escarpments in the atmospheric surface layer due to the localised wind speed up effects such features produce. Wind flow in the vicinity of such topographical features is highly complex with flow separation occurring adjacent to regions of high shear. The current one-dimensional numerical models used by the wind industry in their planning process are unable to predict flow separation. Turbines placed within the recirculation region atop of a cliff will be subjected to fluctuating loads and high vertical shear forces due to the turbulent nature of the flow. Optimal turbine placement beyond the highly distorted recirculation region will ensure estimated power production is achieved, while not subjecting the turbine to unknown fluctuating loads.

There have been a number of works dealing with obstacles immersed in turbulent boundary layers. The majority of these have concentrated on flow over a backward facing step (BFS) and a comprehensive review of these studies can be found in Eaton and Johnston (1981). Studies dealing with separating and reattaching flow over a forward facing isolated step (FFS) are less numerous, most probably due to the unsteady nature of the flow and the presence of two recirculation regions (Eaton and Johnston, 1981). In addition researchers also face difficulty in obtaining accurate data in the recirculation region and attributing flow behaviour to an individual flow parameter due to the dependence of results on a large number of flow parameters (Bradshaw and Wong, 1972). The flow over a FFS has a number of unique features that are shown in Fig. 1. The turbulent boundary layer approaches the obstacle from left to right. The blockage of the step causes an adverse pressure gradient, with the consequence that the flow separates at $\sim 1-1.2h$ upstream of the step and reattaches to the vertical step wall at $\sim 0.6h$ above the ground surface (Leclercq et al., 2001). The upstream recirculation region contains near stagnant fluid which acts as an 'equivalent' slope angle (Bowen and Lindley, 1977).

The blunt leading edge of the FFS acts as the sole fixed separation point for this geometry. A recirculation occurs behind the step, extending from the leading edge to the reattachment point, denoted as X_L. Hence, a strong shear layer develops between the low velocity reverse flow close to the wall and the mean free stream flow, increasing local mixing and the turbulent intensity within the boundary layer. As the step height becomes much larger than the boundary layer thickness (*i.e.* $\delta/h \ll 1$), the geometry resembles that of a blunt flat plate. It is known that in the case of a blunt flat plate, the free stream turbulence level significantly influences the reattachment length although this mechanism remains unclear (Hillier and Cherry, 1981). The separation region experiences a weak regular vortex shedding

* Corresponding author.
E-mail address: michael.sherry@monash.edu (M. Sherry).

0167-6105/$ - see front matter © 2010 Elsevier Ltd. All rights reserved.
doi:10.1016/j.jweia.2010.09.003

which leads to an accumulation of vorticity within the recirculation region. This accumulation process sees the region grow in size until a large scale vortex is ejected from the recirculation region with a resulting reduction in recirculation region size and hence reattachment length (Kiya and Sasaki, 1983). The vorticity accumulation process induces a low frequency oscillation of the shear layer. Therefore, the unsteady behaviour of the shear layer implies that the reattachment point also fluctuates (within a 'reattachment zone' as shown in Fig. 1).

The mean reattachment position, X_L, is sensitive to several parameters, such as the body aspect ratios, L/h, W/h, streamwise length and spanwise width to step height ratios, respectively, and the upstream boundary layer thickness to step height ratio, δ/h (Castro, 1979). A sufficiently large model L/h ratio is required to consider the step truly 'isolated'. The three dimensionality of the recirculation region increases with reductions in the W/h aspect ratio (Largeau and Moriniere, 2007). A single dominant parameter affecting X_L is difficult to determine due to the complex coupled relationship between the two separated regions involved in the FFS geometry (Bradshaw and Wong, 1972).

The previous recirculation studies involving a FFS immersed in a turbulent boundary layer can broadly be separated into two categories. Studies are grouped together based on the upstream boundary layer thickness to the step height ratio, δ/h. The two categories are thus for studies conducted with an approaching boundary layer thickness greater than the step height, *i.e.* $\delta/h > 1$ and conversely studies with a boundary layer thickness less than the step height, *i.e.* $\delta/h > 1$. Studies conducted with $\delta/h > 1$ have clearly shown that the reattachment length is heavily dependent on δ/h (Agelinchaab and Tachie, 2008; Arie et al., 1975; Camussi et al., 2008; Castro and Dianat, 1983; Farabee and Casarella, 1986), whereas when $\delta/h < 1$ it seems that the reattachment length is weakly affected by this ratio, and is usually situated around $4h$ to $5h$ depending on Reynolds number (Bergeles and Athanassiadis, 1983; Gasset et al., 2005; Hattori and Nagano, 2010; Largeau and Moriniere, 2007; Moss and Baker, 1980; Zhang, 1994). The reattachment length in previous studies was determined via a variety of different experimental methods including flow visualisation techniques (Arie et al., 1975; Bergeles and Athanassiadis, 1983; Camussi et al., 2008; Castro and Dianat, 1983; Largeau and Moriniere, 2007), hot wire anemometry (Bergeles and Athanassiadis, 1983; Moss and Baker, 1980), surface pressure measurements (Castro and Dianat, 1983; Farabee and Casarella, 1986; Largeau and Moriniere, 2007; Leclercq et al., 2001), laser doppler velocimetry (Leclercq et al., 2001), particle image velocimetry (Agelinchaab and Tachie, 2008; Camussi et al., 2008; Largeau and Moriniere, 2007) and numerical models (Gasset et al., 2005; Hattori and Nagano, 2010; Zhang, 1994). Results from previous researchers are summarised in Table 1.

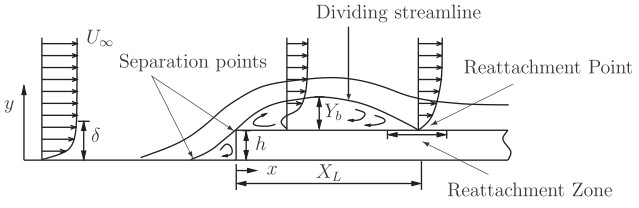

Fig. 1. Flow features over a forward facing step (FFS). Left to right: upstream boundary layer profile, upstream recirculation, step face, recirculation region of present interest, reattachment point.

The purpose of this study is to investigate the velocity fields over a FFS immersed in a turbulent boundary layer for various δ/h ratios over a wide Reynolds number range. Insight into the flow topology above the forward facing step geometry will aid the optimal placement of wind turbines sited within complex terrain.

2. Experimental facilities

The free surface water channel has a working section of $600 \times 800 \times 4000$ mm and a working speed range of $0.09\,\text{m/s} < U_\infty < 0.46\,\text{m/s}$. The channel walls are constructed of glass allowing easy optical access. Flow uniformity is achieved through the use of an upstream honeycomb section and fine turbulence screen. The flow passes through a 3:1 contraction to accelerate the mean flow and reduce the residual streamwise turbulence intensity to 1%.

The experiments were conducted over a wide Reynolds number range, $1400 < Re_h < 19\,000$. The Reynolds number is defined as $Re_h = U_\infty h/\nu$, where U_∞ is the free stream velocity, h is the step height, and ν is the kinematic viscosity of the working fluid. The flow passes through a final turbulence screen situated $16.67h_{\min}$ and $56.67h_{\min}$ upstream of the model leading edge and forward facing step edge, respectively. Here, $h_{\min}$ is the minimum step height of 15 mm. The turbulence screen has a mesh diameter of $0.84h_{\min}$, and a solidity ratio of 22% producing a turbulence level of 1.43%. The final turbulence screen serves to regulate the turbulence level between subsequent measurement days.

A Continuum Minilite PIV (Nd:YAG) laser of wavelength 532 nm was used to produce a pulsed laser sheet of 2 mm thickness. The flow was seeded with polyamide particles of mean diameter 50 μm and specific gravity of $1.06\,\text{g/cm}^3$.

Table 1
Reattachment length results from previous FFS studies including important study parameters, boundary layer height to step height ratio δ/h, step length aspect ratio L/h, and Reynolds number Re_h.

Study	δ/h	L/h	Re_h	X_L
Largeau and Moriniere (2007)	≤ 0.3	≥ 9	$2.88–12.82 \times 10^4$	3.5–5
Hattori and Nagano (2010)	0.33–0.66	23.3	$0.9–3 \times 10^3$	1.82–2.04
Bergeles and Athanassiadis (1983)	0.48	4	2.7×10^4	3.75
Moss and Baker (1980)	0.7	12.7	5×10^4	4.7
Gasset et al. (2005)	~ 0.7	> 6	5×10^4	5.0
Zhang (1994)	0.7	32	–	4.02
Leclercq et al. (2001)	0.7	10	1.7×10^5	3.2
Current study	0.83–2.5	≥ 11.1	$1.4–19 \times 10^3$	1.9–4
Arie et al. (1975)	1.96	4	–	2.5
Farabee and Casarella (1986)	2.4	> 10	2.1×10^4	~ 3
Camussi et al. (2008)	5	> 8	$8.8–26.3 \times 10^3$	1.5–2.1
Castro and Dianat (1983)	5.2	2	5×10^4	1.4
Agelinchaab and Tachie (2008)	9.3	6	1.92×10^3	4.1

Two CCD PIV camera systems with different resolutions were used in conjunction with a 200 mm lens. System one had a maximum resolution of 4008×2672 pixels whilst system two had a maximum resolution of 2004×1336 pixels. The results were invariant of the camera system used. A minimum magnification factor of 50 pixels/mm was employed giving a field of view (FOV) of $5.34h_{\min} \times 3.46h_{\min}$ and $2.67h_{\min} \times 1.73h_{\min}$ for system one and two, respectively. A multi-step interrogation window with an initial size of 64×64 pixels to a final size of 32×32 pixels with 50% overlap was used. This allowed instantaneous velocity maps of 250×167 vectors and 125×83 vectors to be captured for system one and two, respectively. The velocity vector resolution of the velocity maps was 0.64 mm × 0.64 mm. The camera was re-positioned using a manual traversing mechanism with camera alignment ensured prior to data acquisition.

A total of 400 independent image pairs were captured for each spatial position and Reynolds number. The image pairs were captured at 1 Hz so individual velocity realisations are minimally correlated. Whilst the recirculation zone's presented were all the result of averaging of the turbulent flow, convergence (via variance of the fluctuating cross velocity product from the cumulative mean) was shown to occur prior to 400 image pairs. Therefore, 400 images pairs were deemed an acceptable compromise between convergence of the results and excessive use of disc space. A total of 1000 image pairs were used for the POD analysis to allow sufficient data samples in each phase bin. The raw data was processed on a 20 CPU (Beowulf) cluster that allowed rapid analysis of results. Validated cross correlation PIV software developed in-house was employed to generate the displacement fields (Fouras et al., 2008).

3. Experimental model

The experimental model was constructed of acrylic and polycarbonate for rigidity. The step height h, was varied from 15 to 45 mm through the use of perspex spacers giving a L/h and W/h range of 11.1–33.3. The employed aspect ratios, were above the critical aspect ratios to ensure both reattachment to the top surface and that the model is representative of an isolated step in every flow setting ($L/h > 10$) (Castro and Dianat, 1983) and that the flow is nominally two dimensional at mid span ($W/h > 10$) (de Brederode and Bradshaw, 1972).

The model was fitted with end plates to minimise 3D edge effects and all edges bar the FFS leading edge were formed into an asymmetric 5° taper to minimise blockage effects. The maximum blockage ratio (h=45 mm) in the current tests was 9.73%. No corrections were made to adjust the results due to blockage affects. A schematic of the model can be seen in Fig. 2. The model was suspended within the channel in an inverted position. In this configuration, any free surface effects of the water channel were minimised. A boundary layer formed upstream of the step with the profile as shown in Fig. 3. The boundary layer profile was measured at a distance $9h_{\min}$ upstream of the step over the entire

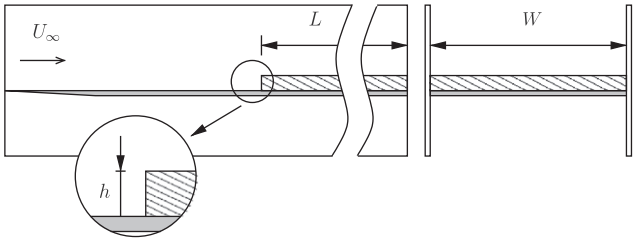

Fig. 2. Schematic of the polycarbonate and acrylic experimental model used in the current study. Height of end is 210 mm.

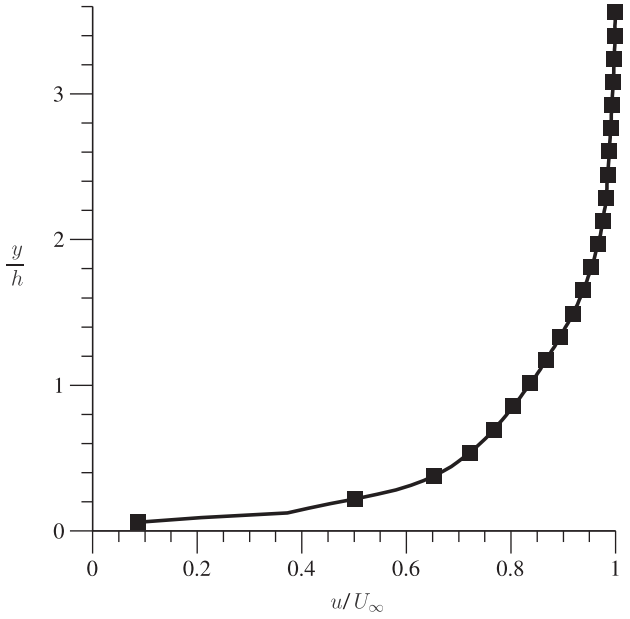

Fig. 3. The upstream boundary layer profile measured at $9h_{h=15\,\mathrm{mm}}$ upstream of the step using 2500 independent PIV images. Only every fifth data point is presented for clarity.

velocity range producing a Reynolds number range of $37\,000 < Re_x < 183\,200$. The boundary layer thickness varied by 10% across this Re_x range, thus it was assumed constant and the maximum thickness was used as a scaling parameter. The boundary layer had a thickness $y = \delta = 2.5h_{\min}$ where $u(y) = 0.99U_\infty$, a shape factor of $H = 1.63$ and a momentum thickness of $0.27h$. The maximum u_{rms} and v_{rms} components within the boundary layer were $\sim 0.2U_\infty$ and $\sim 0.05U_\infty$, respectively. The different step heights gave a δ/h range of $0.83 < \delta/h < 2.5$. A total of 2500 image pairs were utilised for convergence of the boundary layer profile results.

4. Results

The recirculation zone dimensions using the PIV results were determined by calculating the streamlines (see Eq. (1)), above the step surface:

$$\Psi = \int_0^y (\overline{u}/U_\infty)\, \mathrm{d}(y/h), \tag{1}$$

where $\overline{u}$ is the temporal average of the streamwise velocity component. For the data analysis, the Cartesian coordinate system was fixed at the step leading edge. The mean reattachment distance, X_L, occurred where the dividing streamline, $\Psi = 0$, (from here on denoted as Ψ_0) bifurcated at the step surface and the region of negative flow ceased. At the reattachment point, one arm of the dividing streamline returns upstream into the recirculation region and the second continues downstream. The height of the recirculation region is defined as the maximum height of the dividing streamline above the step, Y_b such that $\max(\Psi_0) = \Psi_0(Y_b)$.

A typical mean streamwise velocity, $\overline{u}$, contour line plot obtained from the PIV measurements is shown in Fig. 4. The flow is from left to right, with the length and velocity scales non-dimensionalised against the step height, h, and freestream velocity, U_∞, respectively. The Reynolds number, Re_h of Fig. 4, is 6741. The recirculation region is indicated by the solid line (Ψ_0), while the dashed contour lines depict reverse flow. Further, the region between the largest dashed contour line and the adjacent solid line indicates the mean position of maximum shear within

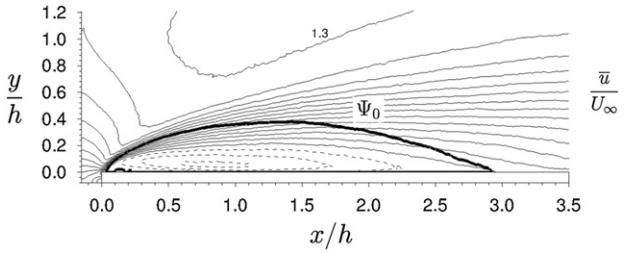

Fig. 4. General bluff body flow features of the FFS flow, contour lines of mean streamwise velocity $\overline{u}$; reference value of 1.3 $\overline{u}/U_\infty$ shown with line increments equal to 0.2 $\overline{u}/U_\infty$; solid line is the dividing streamline Ψ_0, dashed contour lines depict region of entirely negative flow, $\delta/h = 1.25$, $Re_h = 6741$.

the recirculation region. The mean reattachment length, X_L, and the mean height of the recirculation region, Y_b of Fig. 4 are 2.90h and 0.36h, respectively.

Moss and Baker (1980) state that the BFS is the simplest bluff body geometry due to minimum flow deflection of the streamlines. Two instabilities affect the separated region behind a BFS, a convective instability and an absolute instability (Dandois et al., 2007). The convective instability appears in the form of Kelvin–Helmholtz vortices in the free shear layer whereas the absolute instability results in the low frequency flapping of the shear layer (Dandois et al., 2007).

The recirculation zone downstream of a FFS exists in a quasi steady state due to the higher deflection of the incoming flow. While the instability mechanisms affecting a FFS flow were not the primary focus of the current study, some comments can be made regarding the low frequency flapping of the shear layer. The recirculating flow within the separated region is ejected when the region can no longer sustain the amount of entrained fluid. This ejection process causes the free shear layer to flap. This flapping motion causes the reattachment position to oscillate around the mean reattachment position creating a reattachment zone as shown in Fig. 1.

The flapping of the shear layer was investigated using the 'snapshot' proper orthogonal decomposition technique (Sirovich, 1987). The basis of POD is that an input data set can be represented by an orthogonal set of temporal and an orthonormal set of spatial modes. The advantage of POD is that it creates an optimal set of basis functions in terms of energy (here kinetic) within a given flow. We utilised the snapshot POD technique here to perform a spatial kinetic energy decomposition on the fluctuating velocity component. The energy level of the resulting eigenvalues gives an indication of the dominant temporal structures within a flow. The technique has successfully been applied to other bluff body geometries (Kostas et al., 2005; Mathis et al., 2009; van Oudheusden et al., 2005). Using a similar technique as van Oudheusden et al. (2005), the phase angle (ϕ) between the first two temporal eigenvalues ($a_1(t)$ and $a_2(t)$) is calculated, and the resulting distribution binned into eight phases ($\phi = 0, \pi/4, 2\pi/4, \ldots, 7\pi/4$) to determine the spatial structure within the highest energy portion of the flow. The corresponding binned fields were temporally averaged, resulting in the contours of mean streamwise velocity and associated dividing streamlines shown in Fig. 5. In Fig. 5, phase progression is from top to bottom spanning two pages. The contours display the movement of the recirculation region within the two highest energy modes of the flow. Performing a temporal average as in Fig. 4 masks the dynamical movement of the recirculation region. The POD decomposition thus provides further insight into the dynamics of the unsteady recirculation region.

The maximum adverse flow within the recirculation region for the Reynolds number range investigated is between 24 and 36% of

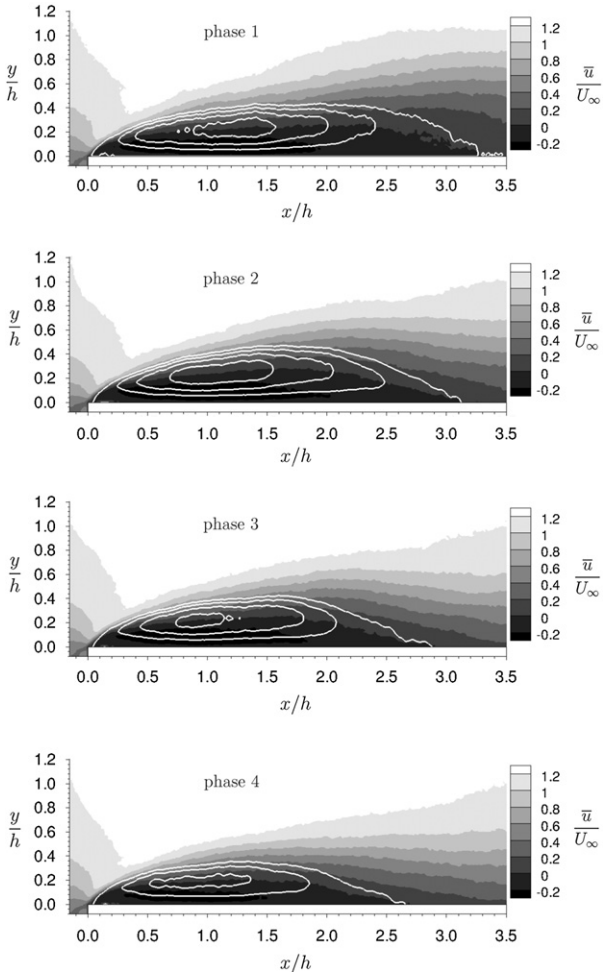

Fig. 5. Eight phase averages from a POD analysis of the FFS shear layer dynamics for $\delta/h = 1.25$, $Re_h = 6\,741$. Phase progression is from top to bottom, 1–4 ($0-3\pi/4$) this page, 5–8 ($\pi-7\pi/4$) on following page, contours of mean velocity $\overline{u}$; white solid streamlines indicate dynamics of recirculation region shape and size.

the freestream velocity. Such a level of adverse flow indicates the cause of the expansion and contraction of the recirculation region shown by the POD results is most likely due to the global instability mode which affects laminar separation bubbles at smaller Reynolds numbers (Castro, 2005). In Fig. 5, the reattachment zone (based on the distribution of phase averaged mean reattachment lengths and recirculation zone heights) extends from 2.36h to 3.28h in the streamwise direction and 0.31h–0.49h in the wall normal direction. The mean reattachment length and mean recirculation zone height (*i.e.* temporal average of all eight phases shown in Fig. 4) for this flow setting are $X_L = 2.90$ and $Y_b = 0.36$ which are $\sim 2\%$ and $\sim 10\%$ different, respectively, to the average reattachment length and recirculation zone height obtained from the dominant POD mode data only. Therefore, the phase decomposition via a POD analysis is an accurate method to capture the dominant flow topology.

The onset of the convective instability—that resulting in the formation of Kelvin–Helmoltz (KH) vortices—was not investigated in the current study.

The free shear layer can be seen from the turbulent velocity component plots of Figs. 6 and 7. Fig. 6 displays the square of the streamwise perturbation field ($\overline{u'u'}/U_\infty^2$) and Fig. 7 displays the non-dimensionalised Reynolds shear stress ($-\overline{u'v'}/U_\infty^2$) component.

It can be seen from the $\overline{u'u'}/U_\infty^2$ field of Fig. 6 that the streamwise Reynolds stresses are generated in the separated

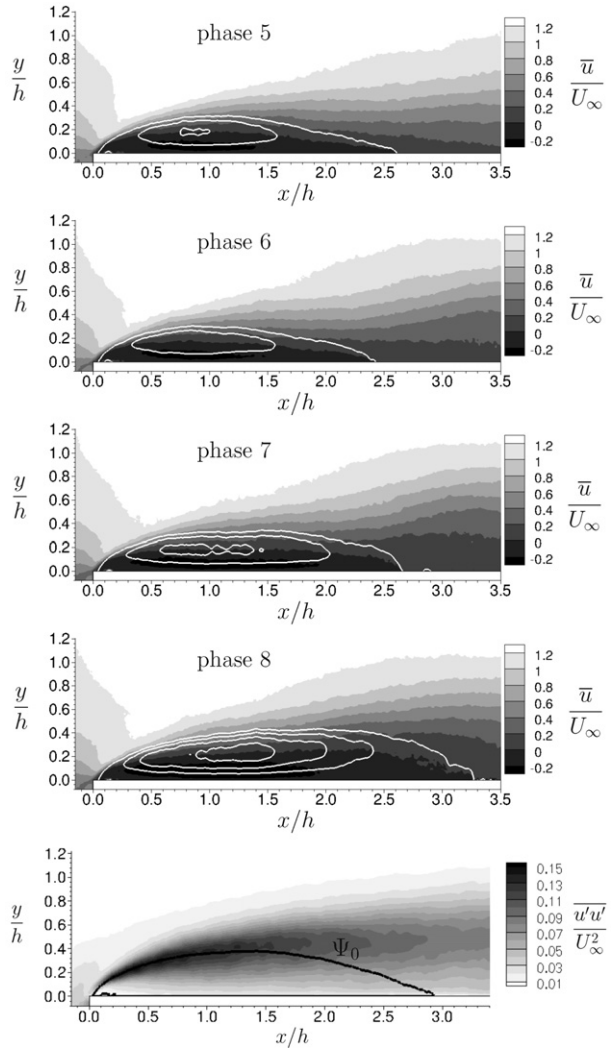

Fig. 6. Streamwise perturbations within the shear layer above a FFS for $\delta/h = 1.25$; $Re_h = 6741$, contours of $\overline{u'u'}/U_\infty^2$; solid line is the dividing streamline Ψ_0.

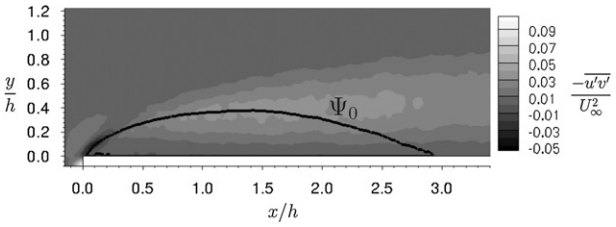

Fig. 7. Reynolds shear stress contours produced above a FFS for $\delta/h = 1.25$; $Re_h = 6741$, contours of $-\overline{u'v'}/U_\infty^2$; solid line is the dividing streamline Ψ_0.

shear layer. This Reynolds stress term has a small magnitude close to the step surface, rises to a peak in the free shear layer before reducing to a low value in the free stream in a similar fashion to that seen in the Moss and Baker (1980) study. At a given streamwise distance downstream from the leading edge, the peak value of this Reynolds stress is located at a similar height to the dividing streamline, Ψ_0 until the dividing streamline curves back toward the step surface. The stress distribution then flattens out and reduces in intensity with downstream distance. The peak stress maximum occurs prior to the streamwise location of the maximum height of the recirculation zone, *i.e.* $\Psi_0(Y_b)$.

The Reynolds shear stress component shown in Fig. 7 has a negative value close to the separation point before changing sign further downstream. The initial negative values of the Reynolds shear stress corresponds to a production region of the Reynolds stress component (Hattori and Nagano, 2010). Positive Reynolds shear stress values arise when velocity fluctuations in the wall normal direction and a positive mean velocity gradient ($\delta\overline{U}/\delta y + \delta\overline{V}/\delta x$) occur (Hattori and Nagano, 2010). In a similar fashion to the streamwise Reynolds stress distribution, the Reynolds shear stress profile also then flattens out and spreads through turbulent mixing.

Turbulent mixing is the principal mechanism promoting reattachment. This mixing entrains higher velocity free stream fluid into the recirculation region to overcome the momentum deficit created by the separation above the step. The maximum streamwise perturbation occurs in the free shear layer just downstream of the step for all Reynolds numbers, a direct result of the bluff nature of the body.

The variation in reattachment length, X_L, with Reynolds number, Re_h, can be seen in Fig. 8. Trends for the three different δ/h ratios are indicated by separate trend lines. It is evident that the variation of X_L with Re_h for a given δ/h ratio (individual trend line) is monotonic over the entire Re_h range. The blockage caused by the step, although different for all three δ/h ratios investigated was at all times less than 10% and so not the source of the variation in X_L with Re_h.

As the Reynolds number increases for a given δ/h ratio, the upstream flow is deflected further into the free stream, elongating the recirculation region. It is known for flow over a blunt flat plate that vortex shedding from the recirculation region occurs above a threshold Reynolds number, $Re_h \sim 800$ (Ota et al., 1981). As the Reynolds number increases past this critical value, the shear layer becomes susceptible to Kelvin–Helmholtz instabilities at intermediate Reynolds numbers (see flow visualisations in Cherry et al., 1984). Fig. 8 reveals the apparent existence of two distinct regimes. In regime 1 ($Re_h \leq 8500$), a linear trend of increasing reattachment length with Reynolds number exists. It is expected that in regime 1, laminar separation occurs from the fixed separation point with transition occurring in the shear layer before turbulent reattachment. In regime 2 ($Re_h \geq 8500$), the reattachment length becomes less sensitive to Reynolds number increases. Regime 2 is an indication that the shear layer transition point moves very close to the fixed separation point such that it could be considered turbulent separation–turbulent reattachment. The regime change is postulated to occur at a lower Reynolds number in forward facing step geometries compared to blunt flat plate geometries due to the turbulent structures within the oncoming boundary layer. As shown by the spread of results

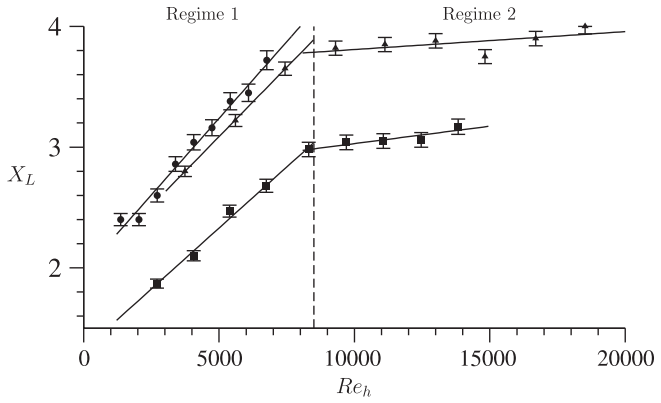

Fig. 8. Variation of X_L with Re_h for three δ/h ratios, $0.83 < \delta/h < 2.5$: •: $\delta/h = 2.5$; ■: $\delta/h = 1.25$; and ▲: $\delta/h = 0.83$.

obtained by previous researchers in Table 1, results are heavily dependent on a number of flow parameters.

The change of regimes may also be due to the flow becoming increasingly three dimensional. It has been shown that flow over a forward facing step becomes increasingly three dimensional with decreases in the W/h ratio (Largeau and Moriniere, 2007). In the current study with the three step heights simulated, the W/h ratio changes by a factor of 3 (whilst at all times remaining >10 ensuring nominally 2D flow).

Increases in W/h ratio produces more 'branching structures' between the upstream and downstream recirculation regions (Largeau and Moriniere, 2007). Unlike the Largeau and Moriniere study, which permitted three dimensional flow around the side of the model, here the experimental models were fitted with end plates which would emphasise this mechanism to transport fluid from the upstream recirculation region to that downstream. As measurements were only taken at the mid span and in one plane, the current results cannot reveal three dimensional fluid movement over the step.

When δ/h is less than unity, the free stream velocity will interact with the leading edge of the step directly. The free stream velocity, being larger than that within the boundary layer, will cause a greater perturbation to the flow field resulting in the flow being deflected further into the free stream. However, the higher free stream velocity above the free shear layer will counteract the increased flow deflection and will limit shear layer expansion. In this way as δ/h becomes much lower than unity ($\delta/h \ll 1$) the influence of the upstream boundary layer is reduced and the results will more closely approximate separated flow over a blunt flat plate (Cherry et al., 1984; Hillier and Cherry, 1981; Ota et al., 1981).

Conversely, when δ/h is greater than unity, the flow will be deflected less into the freestream due to the reduced velocity within the boundary layer. In this case, the reattachment length will be affected significantly by an increase in Reynolds number due to the velocity gradient in the boundary layer. Turbulence within the boundary layer will enhance mixing between the free stream and recirculating flow close to the step, promoting reattachment. It is for this reason that results obtained from $\delta/h>1$ studies are heavily dependent on Re_h, as shown in Table 1. Variance between previous researchers results can be partially be explained by the different boundary layer profiles and length scales therein, which would affect the free shear layer dynamics.

The mean reattachment length obtained by Agelinchaab and Tachie, is higher than any X_L obtained at a comparable Reynolds number in the current study. Free surface effects are an inherent parameter influencing results in water channel studies. A free surface will act as a momentum sink where the flow acceleration created by the step blockage can be released via surface deformation, prolonging separation. Closed channel studies, however, will see a higher velocity and hence greater momentum above the step due to the solid boundaries and the requirement for mass conservation. The higher momentum of the free stream flow will promote turbulent mixing between the flow within the recirculating region and the free stream, leading to earlier reattachment. In the current study, free surface effects of our open channel setup have been minimised through investigating the model in an inverted position.

The model length to height ratio, L/h, is also a controlling factor affecting reattachment to the top surface of a forward facing step (Bergeles and Athanassiadis, 1983; Castro and Dianat, 1983). This value appears heavily dependent on the δ/h ratio simulated. Bergeles and Athanassiadis (1983) showed with a simple flow visualisation method that a minimum L/h ratio of 4 is required for mean shear layer reattachment to the top surface when $\delta/h<1$, whereas Castro and Dianat (1983) determined a minimum L/h of ~ 1.75 to ensure mean shear layer reattachment when $\delta/h>1$. In light of this, a large majority of the previous studies listed in Table 1 were conducted on models where the influence of trailing edge separation on leading edge separation cannot be discounted. It is proposed that the expansion of the test section at the trailing edge of a model will act as a momentum sink promoting reattachment and hence affect the free shear layer dynamics at the leading edge. It is for this reason that recirculation regions can form on the short experimental bodies in Arie et al. (1975), Bergeles and Athanassiadis (1983) and Castro and Dianat (1983) studies.

Further, flow does not reattach to the top surface of the block geometry investigated, in addition to the FFS geometry, in the Moss and Baker study, despite having the same dimensions and being conducted at the same Reynolds number as the Castro and Dianat study. This is clearly a δ/h ratio effect and the mechanism for the difference has been attributed to the turbulence within the boundary layer as outlined earlier. This hypothesis adds another parameter to an already complicated relationship, which contributes to the spread of results in Table 1.

The offset between results at the same Reynolds number in Fig. 8 is due to a combined effect of the upstream flow conditions, principally the boundary layer thickness and body geometry effects.

4.1. Wind turbine placement

Wind turbines are commonly sited in complex terrain to take advantage of the wind speed-up effects the terrain produces. Fig. 4 displays the region of increased wind speed above the step, beneficial in a wind energy sense. The maximum power available to a wind turbine through a given area increases with the cube of the mean wind speed:

$$P_{\max} = \tfrac{1}{2}\rho A U_{\infty}^3, \tag{2}$$

where A is the turbine swept area. From Eq. (2) it follows that a slight increase in wind speed can lead to significant additional energy generation.

The degree of advantage of turbines placed in complex terrain in an energy yield sense can be ascertained through the amplification factor, A_z, defined as the ratio of the wind speed above the topology to that at the same height above flat ground:

$$A_z = \frac{u(x,z)}{u(x_0,z)}. \tag{3}$$

The amplification factor can also be viewed as a power production multiplier for a turbine situated in complex terrain compared against a turbine sited on uniform ground. Rearranging Eq. (2), we obtain

$$P_{\max_c} = A_z^3 P_{\max_u}, \tag{4}$$

where $P_{\max_c}$ is the maximum power available to a wind turbine sited in complex terrain, $P_{\max_u}$ is the power available to the same turbine sited in uniform terrain and A_z, is the amplification factor.

An amplification factor contour map for a δ/h ratio of 1.25 is shown in Fig. 9. The dashed line in Fig. 9 depicts where A_z has a unit value. The maximum amplification factor in Fig. 9 is located very near the step surface ($y/h=0.044$) above the fixed separation point in the region of high shear. The magnitude of the maximum amplification factor is largely Reynolds number independent with a value between 7 and 8. The magnitudes of amplification factor at larger y/h ratios ($y/h>0.2$) are consistent with previous studies above a forward facing step (Bowen and Lindley, 1977). However, the shape of the contour line plot presented in Bowen and Lindley (1977) study (Fig. 4a) is different to Fig. 9 here due to the large δ/h

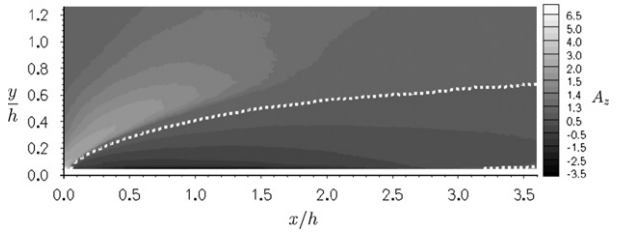

Fig. 9. Contours of the amplification factor, A_z above a FFS for $\delta/h = 1.25$; $Re_h = 6741$. Dashed line indicates position where A_z has a unit value.

ratio ($\delta/h = 20$) simulated. Such a large δ/h ratio will restrict the formation of a recirculation region and alter the dynamics of the free shear layer above the step surface.

Whilst placing turbines in complex terrain is beneficial in a wind energy sense, *i.e.* $P_{\max_c} > P_{\max_u}$ in Fig. 9, complex terrain produces regions of high shear and turbulence as shown in Figs. 6 and 7. The fluctuating loads these regions will induce on turbine components make it difficult to quantify the fatigue loading a turbine will experience during its serviceable lifetime. These regions are therefore undesirable as a wind energy installation site and a compromise must be reached between higher energy yields and detrimental fluctuating loads.

Whilst the Reynolds numbers simulated in the current investigation differ to those found in the field by several orders of magnitude an example of optimal turbine placement can be estimated from Figs. 6, 7 and 9. Ensuring the minimum position of any blade tip is greater than $0.6h$ where h is the cliff height, will result in increased power production due to A_z while restricting detrimental effects of turbulence on turbine components within the shear layer.

5. Conclusions

The recirculation region formed downstream of a forward facing step immersed in a turbulent boundary layer has been investigated using the particle image velocimetry technique. The principal dimension of the recirculation region, the reattachment length, X_L, has been obtained for a wide Reynolds number range and several boundary layer thickness to step height ratios, δ/h.

The reattachment length tended to increase with Reynolds number for a given δ/h ratio. The range of reattachment lengths obtained in the current study was $1.9h < X_L < 4h$. Two regimes were found to exist in the results. The first regime exists for Reynolds numbers less than approximately 8500, where the reattachment length is heavily dependent on the Reynolds number. In the second regime, which exists for Reynolds numbers greater than 8500, the reattachment length is only weakly affected by Reynolds number. Surprisingly, this regime change occurred independently of the δ/h ratio. The regime change is postulated to occur due to shear layer transition immediately after separation and a change in the dynamic between the recirculation regions upstream and downstream of the step. The planar nature of the experimental technique employed here could not reveal this change and may form part of the ongoing work in the area.

The offset between results at the same Reynolds number is due to a combined effect of the upstream flow conditions, principally the boundary layer thickness and body geometry effects. The enhanced local mixing produced by the shear layer above the step and the elevated turbulence intensity within the boundary are thought to be the primary mechanisms promoting reattachment. The complexity of forward facing step flow was highlighted by the dependence of the mean reattachment length, X_L, on a number of flow parameters.

Clearly, these results confirm that wind engineers would be well-advised to consider the flow separation and increased turbulence that complex topographic features produce when siting turbines in complex terrain.

References

Agelinchaab, M., Tachie, M., 2008. PIV study of separated and reattached open channel flow over surface mounted blocks. Journal of Fluids Engineering 130, 1–9.
Arie, M., Kiya, M., Tamura, H., Kosugi, M., Takaoka, K., 1975. Flow over rectangular cylinders immersed in a turbulent boundary layer. Bulletin of the Japan Society of Mechanical Engineers (JSME) 18 (125), 1269–1276.
Bergeles, G., Athanassiadis, N., 1983. The flow past a surface-mounted obstacle. Journal of Fluids Engineering 105, 461–463.
Bowen, A., Lindley, D., 1977. A wind-tunnel investigation of the wind speed and turbulence characteristics close to the ground over various escarpment shapes. Boundary-Layer Meteorology 12, 259–271.
Bradshaw, P., Wong, F., 1972. The reattachment and relaxation of a turbulent shear layer. Journal of Fluid Mechanics 52 (1), 113–135.
Camussi, R., Felli, M., Pereira, F., Aloisio, G., Marco, A.D., 2008. Statistical properties of wall pressure fluctuations over a forward-facing step. Physics of Fluids 20, 075113-1–075113-13.
Castro, I., 1979. Relaxing wakes behind surface-mounted obstacles in rough wall boundary layers. Journal of Fluid Mechanics 93, 631–659.
Castro, I., 2005. The stability of laminar symmetric separated wakes. Journal of Fluid Mechanics 532, 389–411.
Castro, I., Dianat, M., 1983. Surface flow patterns on rectangular bodies in thick boundary layers. Journal of Wind Engineering and Industrial Aerodynamics 11, 107–119.
Cherry, N., Hillier, R., Latour, M., 1984. Unsteady measurements in a separated and reattaching flow. Journal of Fluid Mechanics 144, 13–46.
Dandois, J., Garnier, E., Sagaut, P., 2007. Numerical simulation of active separation control by a synthetic jet. Journal of Fluid Dynamics 574, 25–58.
de Brederode, V., Bradshaw, P., 1972. Three-dimensional flow in nominally two-dimensional separated bubbles. i. Flow behind a rear-ward facing step. Report 72-19, Imperial College of Science and Technology.
Eaton, J., Johnston, J., 1981. A review of research on subsonic turbulent flow reattachment. American Institute of Aeronautics and Astronautics Journal 19, 1093–1100.
Farabee, T., Casarella, M., 1986. Measurements of fluctuating wall pressure for separated/reattached boundary layer flows. Journal of Vibration, Acoustics, Stress, and Reliability in Design 108, 301–307.
Fouras, A., Lo Jacono, D., Hourigan, K., 2008. Target-free stereo PIV: a novel technique with inherent error estimation and improved accuracy. Experiments in fluids 44, 317–329.
Gasset, N., Poitras, G., Gagnon, Y., Brothers, C., 2005. Study of atmospheric boundary layer flows over a coastal cliff. Wind Engineering 29 (1), 3–24.
Hattori, H., Nagano, Y., 2010. Investigation of turbulent boundary layer over forward-facing step via direct numerical simulation. International Journal of Heat and Fluid Flow 31, 284–294.
Hillier, R., Cherry, N., 1981. The effects of stream turbulence on separation bubbles. Journal of Wind Engineering and Industrial Aerodynamics 8, 49–58.
Kiya, M., Sasaki, K., 1983. Structure of a turbulent separation bubble. Journal of Fluid Mechanics 137, 83–113.
Kostas, J., Soria, J., Chong, M., 2005. A comparison between snapshot pod analysis of PIV velocity and vorticity data. Experiments in Fluids 38, 146–160.
Largeau, J., Moriniere, V., 2007. Wall pressure fluctuations and topology in separated flows over a forward facing step. Experiments in Fluids 42, 21–40.
Leclercq, D., Jacob, M., Louisot, A., Talotte, C., 2001. Forward–backward facing step pair: aerodynamic flow wall pressure and acoustic characterisation. Proceedings of the Seventh AIAA/CEAS Aeroacoustics Conference, vol. 1249; 2001, pp. 075113-1–075113-13.
Mathis, R., Lebedev, A., Collin, E., Delville, J., Bonnet, J., 2009. Experimental study of transient forced turbulent separation and reattachment on a bevelled trailing edge. Experiments in Fluids 46, 131–146.
Moss, W., Baker, S., 1980. Re-circulating flows associated with two-dimensional steps. Aeronautical Quarterly (August), 151–172.
Ota, T., Asano, Y., Okawa, J., 1981. Reattachment length and transition of the separated flow over blunt flat plates. Bulletin of the Japan Society of Mechanical Engineers 24 (192), 941–947.
Sirovich, L., 1987. Turbulence and the dynamics of coherent structures. Quarterly of Applied Mathematics 45, 561–590.
van Oudheusden, B., Scarano, F., van Hinsberg, N., Watt, D., 2005. Phase-resolved characterisation of vortex shedding in the near wake of a square-section cylinder at incidence. Experiments in Fluids 39, 86–98.
Zhang, C., 1994. Numerical predictions of turbulent recirculating flows with a $k-\varepsilon$ model. Journal of Wind Engineering and Industrial Aerodynamics 51, 177–201.